Available online at www.sciencedirect.com
SCIENCE DIRECT®
Journal of Solid State Chemistry 178 (2005) 3117–3129
JOURNAL OF SOLID STATE CHEMISTRY
www.elsevier.com/locate/jssc

Solid state synthesis, structures and redox properties of the new $[Mo_6Br^i_7Te^iBr^a_6]^{3-}$ and $[Mo_6Br^i_7Se^iBr^a_6]^{3-}$ octahedral cluster units: Crystallochemistry of the $Rb_{2+x}Mo_6Br^i_{8-x}Y^i_xBr^a_6$ series ($x = 0.5$ for $Y = Te$; $0.25 \leqslant x \leqslant 0.7$ for $Y = Se$) and $Rb_2Mo_6Br_{14}$

Kaplan Kirakci[a], Stéphane Cordier[a,*], Olivier Hernandez[a], Thierry Roisnel[a], Frédéric Paul[b], Christiane Perrin[a]

[a]*Laboratoire de Chimie du Solide et Inorganique Moléculaire, UMR 6511 CNRS-Université de Rennes 1, Institut de Chimie de Rennes, Avenue du Général Leclerc, 35042 Rennes Cedex, France*
[b]*Laboratoire Organométallique et Catalyse: Chimie et Electrochimie Moléculaire, UMR 6509 CNRS-Université de Rennes 1, Institut de Chimie de Rennes, Avenue du Général Leclerc, 35042 Rennes Cedex, France*

Received 4 May 2005; received in revised form 22 July 2005; accepted 26 July 2005
Available online 25 August 2005

Abstract

The solid state synthesis and the structure of the $Rb_2Mo_6Br^i_8Br^a_6$ bromide ($C2/c$, $a = 20.376(5)$ Å, $b = 15.297(5)$ Å, $c = 9.757(5)$ Å, $\beta = 115.969(5)^\circ$, $Z = 4$, $R_1 = 0.037$; w$R_2 = 0.057$) and $Rb_{2+x}Mo_6Br^i_{8-x}Y^i_xBr^a_6$ chalcohalides built up from molybdenum octahedral clusters ($x = 0.5$ for $Y = Te$; $0.25 \leqslant x \leqslant 0.7$ for $Y = Se$) are presented. The crystallochemistry results are based on combined single-crystal and powder X-ray diffraction investigations from several preparations with different loaded compositions. A continuous solid state solution is evidenced between the two limit compositions $Rb_{2.25}Mo_6Br_{13.75}Se_{0.25}$ (*Pn*-3, $a = 13.999(2)$ Å, $Z = 4$, $R_1 = 0.039$; w$R_2 = 0.058$) and $Rb_{2.7}Mo_6Br_{13.3}Se_{0.7}$ (*Pn*-3, $a = 14.144(2)$ Å, $Z = 4$, $R_1 = 0.029$; w$R_2 = 0.048$). On the other hand, in the case of tellurium (data: $Rb_{2.5}Mo_6Br_{13.5}Te_{0.5}$, *Pn*-3, $a = 14.0936(5)$ Å, $Z = 4$, $R_1 = 0.028$; w$R_2 = 0.048$) no solid state solution is observed as previously reported for $Rb_{2.5}Re_6S_{6.5}Cl_{7.5}$ and $K_{2.5}Re_6S_{6.5}Br_{7.5}$. The structural features that act in the stabilization of the new $[Mo_6Br_{13}Y]^{3-}$ units ($Y = Se$, Te) are evidenced and discussed by comparison with those obtained for related compounds in particular in $Rb_{2.5}Re_6S_{6.5}Cl_{7.5}$, $K_{2.5}Re_6S_{6.5}Br_{7.5}$, and $A_2W_6Br_{14}$ series (A = monovalent cation). The substitution of chalcogen for halogen strongly modifies the intrinsic properties of the M_6L_{14} unit. Indeed, the electrochemistry performed on the $[Mo_6Br_{13}Y]^{3-}$ unit after dissolution of the crude solid samples isolated reveals a new and chemically reversible oxidation process at $E_{1/2} = 0.46$ V vs. SCE for $[Mo_6Br_{13}Se]^{3-}$ whilst a similar oxidation process centred at 0.38 V is observed for $[Mo_6Br_{13}Te]^{3-}$.

Keywords: Mo_6 cluster compound; Halide; Chalcogenide; Solid state synthesis; Crystal structure

1. Introduction

The molybdenum octahedral cluster chemistry is based on $[(Mo_6L^i_8)L^a_6]$ units in which the Mo_6 cluster is face-capped by eight inner ligands (L^i) and additionally bonded to six apical ones (L^a) (^{a} = apical, ^{i} = inner according to the Schäfer and Schnering notation [1]). Such units are stabilized for 24 valence electrons per cluster (VEC). Crystal structures of Mo_6 compounds are built up from units that are either discrete or interconnected by shared inner and/or apical ligands [1–2]. Recently, we have entered the field of the molybdenum octahedral cluster chalcohalide chemistry, synthesized by solid state chemistry techniques, containing discrete $[(Mo_6X_{8-x}Y_x)X_6]^{n-}$ units with the following formula:

*Corresponding author. Fax: +33 2 23 23 67 99.
E-mail address: Stephane.Cordier@univ-rennes1.fr (S. Cordier).

0022-4596/$ - see front matter © 2005 Elsevier Inc. All rights reserved.
doi:10.1016/j.jssc.2005.07.026

$A_y[(Mo_6X_{8-x}Y_x)X_6]$ with A = cation, X = halogen, Y = chalcogen [3]. The aim of this work is to control the chalcogen/halogen *ratio* and consequently the charge of the $[(Mo_6X_{8-x}Y_x)X_6]^{n-}$ final anionic unit in the $A_y[(Mo_6X_{8-x}Y_x)X_6]$ series through the choice of counter cation and its loaded stoichiometry. After dissolution, this type of anions could further be involved in coordination chemistry for the design of new molecular materials [4] or compounds with extended open frameworks [5]. Interestingly, the substitution of chalcogen for halogen enables the modification of the electronic properties of the Mo_6L_{14} unit and in particular the decrease of their oxidation potentials [6–8]. Recently, we have isolated the $Cs_4Mo_6Br^i_6Y^i_2Br^a_6$ (Y = S and Se) series based on $[(Mo_6Br^i_6Y^i_2)Br^a_6]^{4-}$ units [3], in which chalcogen and bromine atoms are randomly distributed on the inner positions. Subsequently, cyano $[(Mo_6Br^i_6Y^i_2)(CN)^a_6]^{4-}$ substituted units have been obtained by the interaction of the $Cs_4Mo_6Br^i_6Y^i_2Br^a_6$ solid state precursor with aqueous solution of KCN [3]. Attempts to obtain the '$Cs_3Mo_6Br_{13}Y$'series based on $[(Mo_6Br^i_7Y^i_1)Br^a_6]^{3-}$ units have been unfruitful. In the present work, we present the synthesis and crystallochemistry of the $Rb_2Mo_6Br^i_8Br^a_6$ bromide and $Rb_{2+x}Mo_6Br^i_{8-x}Y^i{}_xBr^a_6$ chalcohalides built up from molybdenum octahedral clusters ($x = 0.5$ for Y = Te; $0.25 \leqslant x \leqslant 0.7$ for Y = Se). The $Rb_2Mo_6Br^i_8Br^a_6$ bromide is based on $[Mo_6Br^i_8Br^a_6]^{2-}$ units whilst the $Rb_{2.5}Mo_6Br^i_{7.5}Te^i_{0.5}Br^a_6$ and $Rb_{2+x}Mo_6Br^i_{8-x}Se^i{}_xBr^a_6$ ($0.25 < x < 0.7$) chalcobromides are based on a mixture of $[Mo_6Br^i_8Br^a_6]^{2-}$ and $[Mo_6Br^i_7Y^iBr^a_6]^{3-}$ units. The phase breadth of the $Rb_{2+x}Mo_6Br^i_{8-x}Se^i{}_xBr^a_6$ series is studied by combined single-crystal and powder X-ray diffraction investigations from several preparations with different loaded compositions. The structural features that act in the stabilization of the new $[Mo_6Br_{13}Y]^{3-}$ units (Y = Se, Te) are evidenced and discussed by comparison with those obtained for related compounds in particular in $Rb_{2.5}Re_6S_{6.5}Cl_{7.5}$ [9], $K_{2.5}Re_6S_{6.5}Br_{7.5}$ [10], and $A_2W_6Br_{14}$ bromides [11].

Cyclic Voltammetry reveals a reversible 24/23 electrons process at $E_{1/2} = 0.46$ V vs. Standard Calomel Electrode (SCE) for $[Mo_6Br_{13}Se]^{3-}$ and at 0.38 V vs. SCE for $[Mo_6Br_{13}Te]^{3-}$.

2. Experimental part

2.1. Synthesis

2.1.1. Synthesis of $Rb_2Mo_6Br_{14}$

First, $MoBr_3$ tribromide was obtained by reaction of molybdenum powder (Plansee, 99.95) in Br_2 flow (Prolabo, technique) at 680 °C. $MoBr_2$ was then prepared by decomposition of $MoBr_3$ at 680 °C under N_2 flow [12]. $Rb_2Mo_6Br_{14}$ was synthesized from a stoichiometric mixture of RbBr (Alfa Aesar 99.9%) and $MoBr_2$ according to the same procedure described for the synthesis of $Cs_2Mo_6Br_{14}$ [13] substituting RbBr for CsBr. Single-crystals suitable for X-ray diffraction studies were obtained directly during such syntheses.

2.1.2. Synthesis of $Rb_{2+x}Mo_6Br^i_{8-x}Y^i{}_xBr^a_6$ series

Typically, a powdered mixture (0.5 g) of RbBr, Mo, $MoBr_2$ and Y (Y = Te (Alfa Aesar 99.9%), Se (Alfa Aesar 99.99%)) was ground, formed as a pellet and placed into a silica tube. Once sealed under vacuum, the tube was heated for 3 days at 900 °C. Single-crystals of $Rb_{2.5}Mo_6Br_{13.5}Te_{0.5}$ and $Rb_{2.7}Mo_6Br_{13.3}Se_{0.7}$ have been initially obtained from reactions designed to synthesize the stoichiometric chalcobromide with the following formula: '$Rb_3Mo_6Br_{13}Y$'. After preliminary structural determinations, by single-crystal X-ray diffraction technique, several syntheses were performed with various '$Rb_{2+x}Mo_6Br^i_{8-x}Y^i{}_xBr^a_6$' loaded compositions in order to determine whether the $Rb_{2.5}Mo_6Br_{13.5}Te_{0.5}$ and $Rb_{2.7}Mo_6Br_{13.3}Se_{0.7}$ stoichiometries, found in these preliminary studies, correspond to definite compositions or whether they correspond to a particular composition within phase breadths. In the '$Rb_{2+x}Mo_6Br^i_{8-x}Y^i{}_xBr^a_6$' loaded compositions, the rubidium and chalcogen contents were adjusted to maintain a VEC value of 24 on the Mo_6 cluster, that corresponds to a full electronic occupation of the Mo–Mo bonding levels of the Mo_6L_{14} molecular orbital diagram [2]. Consequently, such compositions correspond to compounds built up from $[M_6Br^i_{8-x}Y^i{}_xBr^a_6]^{(2+x)-}$ average anionic units—corresponding to a mixture of $(1-x)[Mo_6Br_{14}]^{2-}$ with $x[Mo_6Br_{13}Y]^{3-}$—associated with $(2+x)$ Rb^+ counter cations. In order to homogenize the powders and to increase the yield of reaction, after a first heating, the compounds were ground in inert atmosphere and heated once more at the same temperature for 3 days. The single-crystals for X-ray diffraction investigations were all issued from syntheses of the first heating since the single-crystals issued from the second heating were too small for such investigations. As discussed below, combined single-crystal and powder X-ray diffraction investigations of the resulting products revealed a phase breadth for the $Rb_{2+x}Mo_6Br^i_{8-x}Se^i{}_xBr^a_6$ series (with $0.25 \leqslant x \leqslant 0.7$) and a defined composition for $Rb_{2.5}Mo_6Br^i_{7.5}Te^i_{0.5}Br^a_6$.

2.2. Energy dispersive spectrometry (EDS) analysis

Elemental content has been determined first by chemical analyses of single-crystals at the "Centre for Scanning Electron Microscopy and Microanalyses of Rennes 1 University, France" by Energy Dispersive Spectrometry (EDS) using a scanning electron microscope JEOL JSM 6400 equipped with a microprobe EDS OXFORD LINK ISIS. The atomic percentages obtained for several single-crystals for $Rb_2Mo_6Br_{14}$

were: Rb: 8%, Mo: 31%, Br: 61% (theoretical Rb: 9%, Mo: 27.27%, Br: 63.63%). Analysis performed on several selected single-crystals of $Rb_{2.5}Mo_6Br^i_{7.5}Te^i_{0.5}Br^a_6$ from several '$Rb_{2+x}Mo_6Br^i_{8-x}Te^i{}_xBr^a_6$' preparations showed that they all contained the expected elements and that they exhibit the same loaded compositions with the following atomic percentages: Rb: 12, Mo: 29, Br: 56, Te: 3 (theoretical for $Rb_{2.5}Mo_6Br^i_{7.5}Te^i_{0.5}Br^a_6$: Rb: 11.11, Mo: 26.66, Br: 60, Te: 2.22). The refined cell parameters determined afterwards on these single-crystals did not deviate within the s.u.'s corroborating a definite composition. Contrary to what has been observed for $Rb_2Mo_6Br_{14}$ and $Rb_{2.5}Mo_6Br^i_{7.5}Te^i_{0.5}Br^a_6$, the EDS analysis performed on selected single-crystals of '$Rb_{2+x}Mo_6Br^i_{8-x}Se^i{}_xBr^a_6$' series revealed some fluctuations in the composition depending on the loaded one. However, for several single-crystals from the '$Rb_{2.5}Mo_6Br^i_{7.5}Se^i_{0.5}Br^a_6$' loaded composition, the elemental analysis gave the following results: Rb: 11, Mo: 27, Br: 60, Se: 2 (theoretical for $Rb_{2.5}Mo_6Br^i_{7.5}Se^i_{0.5}Br^a_6$: Rb: 11.11, Mo: 26.66, Br: 60, Se: 2.22). The cell parameters of the analysed single-crystals, determined by X-ray diffraction, do not deviate from 14.070(5) Å within the s.u.'s in agreement with the $Rb_{2.5}Mo_6Br^i_{7.5}Se^i_{0.5}Br^a_6$ composition found by single X-ray diffraction analysis. Single-crystals from other '$Rb_{2+x}Mo_6Br^i_{8-x}Se^i{}_xBr^a_6$' ($x \neq 0.5$) loaded compositions revealed fluctuations in the final compositions. In order to determine the range of homogeneity, it was decided to collect single-crystal for high and low x '$Rb_{2+x}Mo_6Br^i_{8-x}Se^i{}_xBr^a_6$' loaded compositions. A single-crystal of $Rb_{2.7}Mo_6Br^i_{7.3}Se^i_{0.7}Br^a_6$ was collected in a preparation with a '$Rb_3Mo_6Br^i_7Se^iBr^a_6$' loaded composition. The structure has been determined and afterwards an EDS analysis has been performed leading to the following results: Rb: 13, Mo: 29, Br: 54, Se: 3 (theoretical for $Rb_{2.7}Mo_6Br^i_{7.3}Se^i_{0.7}Br^a_6$: Rb: 11.89, Mo: 26.43, Br: 58.59, Se: 3.08). A same procedure has been performed for $Rb_{2.25}Mo_6Br^i_{7.75}Se^i_{0.25}Br^a_6$ but for a lower x loaded composition ($x = 0.25$). As stressed below, it turns out that the x composition exhibits a linear variation versus the a parameter. This evolution is the consequence of the correlation between the Rb, Br and Se contents in order to maintain a 24 VEC value on the Mo_6 cluster.

2.3. Diffraction studies

2.3.1. Single-crystal X-ray diffraction studies

Single-crystal X-ray diffraction data of $Rb_2Mo_6Br_{14}$, $Rb_{2.5}Mo_6Br_{13.5}Te_{0.5}$ and $Rb_{2+x}Mo_6Br_{14-x}Se_x$ (with the following final refined x value: 0.24(1), 0.48(1) and 0.69(1)) were collected at room temperature on a Nonius KappaCCD area-detector X-ray diffractometer with Mo K_α radiation ($\lambda = 0.71069$ Å) (Centre de Diffractométrie de l'Université de Rennes 1, France). Details of data collections and structure refinements are reported in Tables 1 and 2. The data processing was performed by the EvalCCD analysis software [14] and an absorption correction was made through SADABS program [15]. The calculation of E-statistics performed on the data suggested a centrosymmetric space group for all compounds [16]. Among the possible space groups deduced from the observed systematic extinctions, the refinement procedure allowed to retain unambiguously

Table 1
Crystallographic data for the structure determinations of $Rb_2Mo_6Br_{14}$ and $Rb_{2.5}Mo_6Br_{13.5}Te_{0.5}$

Empirical formula	$Rb_2Mo_6Br_{14}$	$Rb_{2.44(1)}Mo_6Br_{13.63(2)}Te_{0.37(2)}$
Formula weight	1865.32	1920.56
Space group	$C2/c$ No. 15	Pn-3 No. 201
a (Å)	20.376(5)	14.0936(5)
b (Å)	15.297(5)	
c (Å)	9.757(5)	
β (°)	115.969(5)	
V (Å^3)	2734 (2)	2799.4(2)
Z	4	4
D_{calc} (g cm^{-3})	4.531	4.557
Crystal dimensions (mm^3)	$0.078 \times 0.098 \times 0.117$	$0.063 \times 0.066 \times 0.110$
Total reflections collected	17195	37655
Unique reflections	4741	1079
R_{int} (all reflections)	0.0588	0.0767
μ (mm^{-1})	26.655	26.645
T (°C)	20	20
λ (Å)	0.71069	0.71069
Observed reflections [$I > 2\sigma$ (I)]	3146	908
Refined parameters	106	43
R_1,[a] [$I > 2\sigma(I)$]	0.037	0.0285
wR_2,[a] all data	0.0568	0.0477
$\Delta\rho_{min}/\Delta\rho_{max}$ (e Å^{-3})	−0.997/1.413	−1.404/1.325

[a] $R_1 = \sum_{hkl}|F_o - F_c| / \sum_{hkl}|F_o|$; $wR_2 = [\sum_{hkl}[w(F_o{}^2 - F_c^2)^2] / \sum_{hkl}[w(F_o^2)^2]]^{1/2}$.

Table 2
Crystallographic data for the structure determinations of $Rb_{2.24}Mo_6Br_{13.76}Se_{0.24}$, $Rb_{2.5}Mo_6Br_{13.5}Se_{0.5}$ and $Rb_{2.8}Mo_6Br_{13.3}Se_{0.7}$

Empirical formula	$Rb_{2.24(1)}Mo_6Br_{13.76}Se_{0.24}$	$Rb_{2.48(1)}Mo_6Br_{13.52}Se_{0.48}$	$Rb_{2.69(1)}Mo_6Br_{13.31}Se_{0.69}$
Formula Weight	1885.60	1905.89	1923.64
Space group	*Pn*-3 No. 201	*Pn*-3 No. 201	*Pn*-3 No. 201
a (Å)	13.999(2)	14.0782(3)	14.144(2)
V (Å^3)	2743.4(2)	2791.2(4)	2829.5(5)
Z	4	4	4
D_{calc} (g cm^{-3})	4.565	4.535	4.512
Crystal dimensions (mm^3)	$0.063 \times 0.074 \times 0.092$	$0.056 \times 0.059 \times 0.64$	$0.072 \times 0.074 \times 0.140$
Total reflections collected	35871	31715	31391
Unique reflections	1060	1076	1059
R_{int} (all reflections)	0.1312	0.1210	0.1089
μ (mm^{-1})	26.958	26.882	26.850
T (°C)	20	20	20
λ (Å)	0.71069	0.71069	0.71069
Observed reflections [$I>2\sigma(I)$]	838	832	792
Refined parameters	38	38	42
R_1,[a] [$I>2\sigma(I)$]	0.0397	0.0335	0.0295
wR_2,[a] all data	0.0585	0.0485	0.0479
$\Delta\rho_{min}/\Delta\rho_{max}$ (e Å^{-3})	−1.225/1.324	−1.193/0.985	−0.771/0.992

[a] $R_1 = \sum_{hkl}|F_o - F_c|/\sum_{hkl}|F_o|$; $wR_2 = [\sum_{hkl}[w(F_o^2 - F_c^2)^2]/\sum_{hkl}[w(F_o^2)^2]]^{1/2}$.

the $C2/c$ centrosymmetric space group for $Rb_2Mo_6Br_{14}$ bromide and the *Pn*-3 centrosymmetric space group for all the chalcobromides. The structures have been solved by direct methods using SIR97 program [17]. Subsequent structural refinements by least-squares techniques, combined with Fourier difference syntheses, were performed using SHELXL-97 program [18].

In $Rb_{2.5}Mo_6Br_{13.5}Te_{0.5}$, an inner ligand position is randomly occupied by bromine and tellurium atoms (Br1 and Te1), whilst the other ligand positions (8*e*, 24*h*) are fully occupied by bromine (Br2, Br3, respectively). In a first step, it was assumed that Br1 fully occupied a 24*h* position but after several cycles of refinements, it turned out that an electronic peak remained close to Br1 at a distance from molybdenum corresponding to a Mo–Te bond length. Tellurium Te1 was then introduced on this residue with the same atomic displacement parameter as Br1. The sum of the occupancies of Br1 and Te1 was restricted to the value corresponding to a fully occupied 24*h* position. Afterwards, the restraint on atomic displacement parameter was relaxed during the convergence, leading to final positions in agreement with reliable Mo–(Br, Te) inter-atomic distances. Owing to the small occupancy of tellurium, this atom was refined isotropically. The final formula deduced from structural determination is $Rb_{2.44(2)}Mo_6Br_{13.63(2)}Te_{0.37(2)}$. It has been rounded to $Rb_{2.5}Mo_6Br_{13.5}Te_{0.5}$ for clarity since this refined formula is very close to the point $x = 0.5$ of the general $Rb_{2+x}Mo_6Br_{14-x}Te_x$ formula considering that the number of VEC is constant and equal to 24.

Although X-ray diffraction techniques are not appropriate to discriminate Se and Br owing to their close scattering factors, these two elements were assumed randomly distributed on all the inner ligand positions (L1 and L2, respectively) for the three $Rb_{2+x}Mo_6Br_{14-x}Se_x$ compositions for which structural determinations have been performed (refined x value: 0.24(1), 0.48(1) and 0.69(1)). This assumption is supported by the close ionic radii for bromine and selenium [19]. Moreover, let us recall that previous results on Mo_6 chalcohalides indicate that Se cannot be located in apical position [20] and in $Rb_{2.5}Re_6S_{6.5}Cl_{7.5}$ and $K_{2.5}Re_6S_{6.5}Br_{7.5}$ related compounds [9,10], halogen and chalcogen atoms have been found randomly distributed on all inner positions. The presence of selenium in the '$Rb_{2+x}Mo_6Br_{14-x}Se_x$' series as well as the variations in atomic composition depending on the x loaded values was firstly established by EDS analysis (see Section 2.2). Furthermore, the number of valence electrons VEC is constant and equal to 24 that implies a correlation between the Rb, Br and Se content. Consequently, the selenium (x) content could also be deduced from that of rubidium ($2+x$) in the $Rb_{2+x}Mo_6Br_{14-x}Se_x$ formula.

The atomic positional parameters and the equivalent displacement parameters of these compounds are reported in Tables 3–6. Relevant interatomic distances for discussion are reported in Tables 7 and 8. Further details of the crystal structure investigation can be obtained from the Fachinformationszentrum Karlsruhe, 76344 Eggenstein-Leopoldshafen, Germany (fax: (49) 7247-808-666; e-mail: crysdata@fiz.karlsruhe.de), on quoting the depository numbers CSD__415564 ($Rb_2Mo_6Br_{14}$), CSD__415565 ($Rb_{2.5}Mo_6Br_{13.5}Te_{0.5}$), CSD__415566 ($Rb_{2.25}Mo_6Br_{13.75}Se_{0.25}$), CSD__415567 ($Rb_{2.5}Mo_6Br_{13.5}Se_{0.5}$) and CSD__415568 ($Rb_{2.7}Mo_6Br_{13.3}Se_{0.7}$), respectively.

Table 3
Positional and equivalent displacement parameters (Å^2) for $Rb_{2.5}Mo_6Br_{13.5}Te_{0.5}$

Atom	Position	x	y	z	Occupancy	U_{eq}
Mo	24*h*	0.53143(3)	0.37894(3)	0.04246(3)	1	0.0259(1)
Te1	24*h*	0.6986(10)	0.3906(12)	0.9521(11)	0.062(4)	0.024(4)[a]
Br1	24*h*	0.69305(12)	0.39012(12)	0.95509(12)	0.938(4)	0.0389(5)
Br2	8*e*	0.36930(4)	0.36930(4)	0.13070(4)	1	0.0489(3)
Br3	24*h*	0.57547(6)	0.20748(4)	0.09799(5)	1	0.0627(2)
Rb1	4*c*	1/2	0	0	1	0.0415(3)
Rb2	6*d*	3/4	1/4	1/4	0.957(4)	0.0522(5)

[a] $U_{eq} = \frac{1}{3}\sum_i\sum_j\left(U^{ij}a^i a^j \vec{a}_i \cdot \vec{a}_j\right)$ except for Te1—refined isotropically—in which case the isotopic displacement parameter is given.

Table 4
Positional and equivalent displacement parameters (Å^2) for $Rb_{2.7}Mo_6Br_{13.3}Se_{0.7}$

Atom	Position	x	y	z	Occupancy	U_{eq}
Mo	24*h*	0.53128(4)	0.37910(3)	0.04212(4)	1	0.0301(1)
L1	24*h*	0.69183(4)	0.39110(5)	0.95410(5)	1	0.0417(2)
L2	8*e*	0.37002(5)	0.37002(5)	0.12998(5)	1	0.0570(4)
Br3	24*h*	0.57548(7)	0.20768(5)	0.09733(6)	1	0.0667(3)
Rb1	4*c*	1/2	0	0	1	0.0502(4)
Rb2	6*d*	3/4	1/4	1/4	1	0.0546(6)
Rb3	8*e*	0.3478(7)	0.1522(7)	0.1522(7)	0.096(5)	0.068(6)

$L = 0.063Se + 0.937Br$.

Table 5
Positional and equivalent displacement parameters (Å^2) for $Rb_{2.5}Mo_6Br_{13.5}Se_{0.5}$

Atom	Position	x	y	z	Occupancy	U_{eq}
Mo	24*h*	0.53139(4)	0.37878(3)	0.04238(4)	1	0.0234 (1)
L1	24*h*	0.69267(4)	0.39075(5)	0.95436(5)	1	0.0338(2)
L2	8*e*	0.36948(5)	0.36948(5)	0.13052(5)	1	0.0456(3)
Br3	24*h*	0.57545(7)	0.20708(5)	0.09794(6)	1	0.0569(3)
Rb1	4*c*	1/2	0	0	1	0.0390(4)
Rb2	6*d*	3/4	1/4	1/4	0.987(5)	0.0521(6)

$L = 0.063Se + 0.937Br$.

Table 6
Positional and equivalent displacement parameters (Å^2) for $Rb_{2.2}Mo_6Br_{13.8}Se_{0.2}$

Atom	Position	x	y	z	Occupancy	U_{eq}
Mo	24*h*	0.53153(4)	0.37838(4)	0.04234(4)	1	0.0255(1)
L1	24*h*	0.69321(5)	0.39030(6)	0.95394(5)	1	0.0355(2)
L2	8*e*	0.36920(5)	0.36920(5)	0.13080(5)	1	0.0457(4)
Br3	24*h*	0.57611(8)	0.20683(6)	0.09826(7)	1	0.0573(3)
Rb1	4*c*	1/2	0	0	1	0.0409(4)
Rb2	6*d*	3/4	1/4	1/4	0.829(6)	0.0501(7)

$L = 0.063Se + 0.937Br$.

2.3.2. *Powder X-ray diffraction studies*

The powder X-ray diffraction patterns of the resulting products from various '$Rb_{2+x}Mo_6Br^i_{8-x}Y^i_xBr^a_6$' loaded compositions were recorded on a BRUKER AXS D8 Advance diffractometer (θ–θ Bragg–Brentano geometry) using a monochromatic Cu$K_{\alpha 1}$ radiation and a Linear Position Sensitive Detector (Braun L-PSD). A whole-powder-pattern profile fitting procedure without structural constraints (Le Bail refinement, Thompson–Cox–Hastings profile function [21]) was used through FullProf/WinPLOTR [22,23] in order to refine the cell as well as the profile parameters. For each powder,

Table 7
Interatomic distances (Å) in $Rb_{2.4}Mo_6Br_{13.6}Te_{0.4}$, $Rb_{2.2}Mo_6Br_{13.8}Se_{0.2}$, $Rb_{2.5}Mo_6Br_{13.5}Se_{0.5}$ and in $Rb_{2.7}Mo_6Br_{13.3}Se_{0.7}$

	$Rb_{2.4}Mo_6Br_{13.6}Te_{0.4}$	$Rb_{2.2}Mo_6Br_{13.8}Se_{0.2}$	$Rb_{2.5}Mo_6Br_{13.5}Se_{0.5}$	$Rb_{2.7}Mo_6Br_{13.3}Se_{0.7}$
	Mo_6 cluster			
Mo1–Mo1	2.6325(7)	2.6234(10)	2.6322(8)	2.6357(9)
Mo1–Mo1	2.6328(8)	2.6264(10)	2.6324(9)	2.6368(8)
	$Mo_6Br_{14-x}Y_x$ unit			
Mo1–Br1	2.594(2)	2.5850(10)	2.5924(8)	2.5953(9)
Mo1–Te1	2.685(2)			
Mo1–Br1	2.607(2)	2.5911(9)	2.5974(8)	2.6002(8)
Mo1–Te1	2.651(2)			
Mo1–Br1	2.623(2)	2.6032(9)	2.6099(8)	2.6105(8)
Mo1–Te1	2.669(2)			
Mo1–Br2	2.605(1)	2.5911(13)	2.5988(11)	2.6006(12)
Mo1–Br3	2.6148(7)	2.6019(10)	2.6154(8)	2.6227(8)
	Rubidium environment			
Rb1–Br3	3.4044(6) × 6	3.3779(8) × 6	3.3958(7) × 6	3.4152(7) × 6
Rb2–Br1	3.591(2) × 4	3.5553(7) × 4	3.5858(6) × 4	3.6046(6) × 4
Rb2–Te1	3.54(2) × 4			
Rb2–Br3	3.3165(7) × 4	3.2869(9) × 4	3.3150(8) × 4	3.3338(8) × 4
Rb3–Br2				3.113(8) × 3
Rb3–Br3				3.404(9) × 3

Table 8
Interatomic distances (Å) in $Rb_2Mo_6Br_{14}$

	$Rb_2Mo_6Br_{14}$
	Mo_6 cluster
Mo1–Mo2	2.6279(9)
Mo1–Mo2	2.6297(8)
Mo1–Mo3	2.6365(8)
Mo1–Mo3	2.6389(15)
Mo2–Mo3	2.6319(8)
Mo2–Mo3	2.6353(10)
	Mo_6Br_{14} unit
Mo1–Br1	2.5940(10)
Mo1–Br2	2.5856(8)
Mo1–Br3	2.5964(10)
Mo1–Br4	2.6070(8)
Mo1–Br6	2.6097(8)
Mo2–Br1	2.6041(8)
Mo2–Br2	2.5948(15)
Mo2–Br3	2.6084(15)
Mo2–Br4	2.6024(8)
Mo2–Br5	2.6233(9)
Mo3–Br1	2.5974(10)
Mo3–Br2	2.5834(10)
Mo3–Br3	2.5970(9)
Mo3–Br4	2.5944(8)
Mo3–Br7	2.5918(11)
	Rubidium environment
Rb1–Br6	3.3721(18) × 2
Rb1–Br6	3.4582(11) × 2
Rb1–Br7	3.4163(10) × 2
Rb2–Br3	3.718(2) × 2
Rb2–Br4	3.672(2) × 2
Rb2–Br5	3.267(2) × 2
Rb2–Br5	3.296(2) × 2
Rb2–Br5	3.322(2) × 2
Rb2–Br5	3.452(2) × 2

all the coexisting phases were introduced, leading to satisfactory profile *Rp*-factors. Subsequently, a Rietveld refinement was carried out in order to evaluate the yield of reaction of the obtained $Rb_{2+x}Mo_6Br^i_{8-x}Y^i_xBr^a_6$ compound versus the loaded stoichiometries (rough quantitative phase analysis). Owing to the complexity of the powder patterns in terms of number of coexisting phases and to the induced high degree of accidental overlapping of diffraction lines, combined with the medium instrumental angular resolution of the PSD, no attempt to refine the atomic parameters were made through this rough analysis, the profile parameters being set to the previously obtained Le Bail refinement values. The evolutions of the unit-cell parameters as well as of the reaction yield versus the loaded composition are reported in Table 9.

The refined *a* parameters obtained by powder X-ray diffraction for the three loaded '$Rb_{2+x}Mo_6Br^i_{8-x}Te^i_xBr^a_6$' compositions ($x = 0.25$, 0.5 and 0.75) are very close within the s.u.'s. They are similar to the value obtained by single-crystal X-ray diffraction for $Rb_{2.5}Mo_6Br^i_{7.5}Te^i_{0.5}Br^a_6$. This feature indicates that $Rb_{2.5}Mo_6Br^i_{7.5}Te^i_{0.5}Br^a_6$ corresponds to a defined composition that is obtained whatever the loaded composition. On the other hand, in the selenium series, the *a* cell parameter of the compounds issued from the three '$Rb_{2+x}Mo_6Br^i_{8-x}Se^i_xBr^a_6$' loaded compositions ($x = 0.25$, 0.5 and 1.25) varies within the range 14.057(1)–14.158(1) Å from the powder diffraction analysis. This range of values is included in that found by single-crystal diffraction investigations (in this instance the *x* values could be refined): 13.999(2)–14.144(2) Å. As one can see in Fig. 7, the evolution of *x* versus *a* parameter for the three

Table 9
Variation of the refined *a* parameter and yield of $Rb_{2+x}Mo_6Br^i_{8-x}Y^i_xBr^a_6$ using X-ray powder diffraction data versus the loaded composition

Loaded composition	'$Rb_{2.25}Mo_6Br^i_{7.75}Te^i_{0.25}Br^a_6$'	'$Rb_{2.5}Mo_6Br^i_{7.5}Te^i_{0.5}Br^a_6$'	'$Rb_{2.75}Mo_6Br^i_{7.25}Te^i_{0.75}Br^a_6$'
a (Å), yield (%)	14.1005(1), 27(2)	14.0998(1), 62(2)	14.1001(1), 44(2)
Loaded composition	'$Rb_{2.25}Mo_6Br^i_{7.75}Se^i_{0.25}Br^a_6$'	'$Rb_{2.5}Mo_6Br^i_{7.5}Se^i_{0.5}Br^a_6$'	'$Rb_{3.25}Mo_6Br^i_{6.75}Se^i_{1.25}Br^a_6$'
a (Å), yield (%)	14.0572(1), 73(2)	14.0743(1), 61(2)	14.1582(1), 32(2)

single-crystals follows a linear law. The *a* parameters obtained after reaction of the three loaded '$Rb_{2+x}Mo_6Br^i_{8-x}Se^i_xBr^a_6$' powder compositions ($x = 0.25$, 0.5 and 1.25) are reported on the straight line (points A, B and C, respectively). The three corresponding *x* values extrapolated from the 'single-crystal' $x(a)$ evolution are 0.42, 0.47 and 0.73, respectively, for the powder samples. The analysis of the results obtained by single-crystal and powder X-ray diffractometry enables to deduce the phase breadth of the seleniobromide with the general formula $Rb_{2+x}Mo_6Br^i_{8-x}Se^i_xBr^a_6$. Indeed, the upper *x* value of the phase breadth is close to $x = 0.7$ whilst the lower *x* value is less than or equal to 0.24, but cannot reach 0 since another structure-type is observed for this value (see $Rb_2Mo_6Br_{14}$, Section 3).

The rough quantitative phase analysis reveals that the yield of reaction of the '$Rb_{2+x}Mo_6Br^i_{8-x}Se^i_xBr^a_6$' series decreases as the *x* value increases. The presence and yield of secondary phases ($Mo_6Br_{10}Se$, $Rb_2Mo_6Br_{14}$, $Rb_4Mo_6Br_{12}Se_2$ or $Rb_{12}Mo_9Br_{31}Se$ [24]) depends on the loaded composition, richer rubidium phases being preferentially formed for high *x* values. In the case of the $Rb_{2+x}Mo_6Br^i_{8-x}Te^i_xBr^a_6$ series, the maximum yield is obviously obtained for the '$Rb_{2.5}Mo_6Br^i_{7.5}Te^i_{0.5}Br^a_6$' loaded composition that corresponds to the stoichiometry of the defined compound. For $x = 0.25$, the main product is $Rb_2Mo_6Br_{14}$ whilst for $x = 0.75$, it is $Rb_{12}Mo_6Br_{31}Te$ [24].

2.4. Electrochemistry

Given the very poor solubility of the isolated solid samples in dichloromethane, the solubility of the crude $Rb_{2.5}Mo_6Br^i_{7.5}Te^i_{0.5}Br^a_6$ extract was however sufficient to record a cyclic voltammogram (supplementary material) from saturated solutions after sonication under an inert atmosphere (nitrogen or argon). Two irreversible waves could be detected around 1.35 and 0.38 V vs. S.C.E., respectively. The first waves correspond to the oxidation of Mo_6Br_{14} and is close to the values reported in the literature [7]. The second wave becomes chemically reversible when the potentials are not scanned above 0.7 V vs. SCE (Fig. 8). It has been attributed to the oxidation of a $Mo_6Te_1Br_{13}$ unit since this range of values has already been observed for other monosubstituted Mo_6 chalcohalides [3,7,8,25]. The $Rb_{2+x}Mo_6Br^i_{8-x}Se^i_xBr^a_6$ selenium series are slightly more soluble in dichloromethane and also exhibit two new waves at 0.46 and 1.13 V vs. SCE (supplementary material), in addition to the irreversible wave around 1.30 V, attributed to the oxidation of '$Mo_6Br^i_8Br^a_6$' [7]. Notably, no distinct reduction peaks are observed in the region as low as –1.2 V vs. SCE in this solvent. Again, at potentials above 1.3 V, clusters undergo an irreversible multielectron oxidation followed by decomposition, along with the passivation of the working electrode. The chemically reversible wave at 0.46 V (Fig. 8) is attributed to the oxidation of a $Mo_6Br_{13}Se_1$ unit by analogy with that observed for $Mo_6Te_1Br_{13}$. The second oxidation wave (1.13 V) has been attributed to a soluble byproduct and more precisely $Rb_{12}Mo_9Br_{31}Se$ [24].

3. Results and discussion

3.1. Crystal structures of $Rb_2Mo_6Br_{14}$

The crystal structure of $Rb_2Mo_6Br_{14}$ is isostructural with those of $Rb_2W_6Br_{14}$ and $Rb_2Mo_6Cl_{14}$ [26]. The Mo_6Br_{14} unit (Fig. 1a) is centred on a -1 site symmetry and exhibits similar interatomic distances as those found in $Cs_2Mo_6Br_{14}$ [13]. The description of $Rb_2W_6Br_{14}$ structure has been previously drawn following 'a *hcp* pattern parallel (100) with the Rb^+ cations between the layers' [11]. This model is partially true since the units are effectively staked according to a *ABAB* succession of units along this direction. However, such a stacking should generate octahedral and tetrahedral sites of units. This feature is in contradiction with the prismatic unit environment of Rb1. The unit layer and unit-cell are represented in Figs. 1b and 2a, respectively. It turns out that the β angle of the monoclinic unit-cell is too far from 90° to consider that the stacking occurs along the [0 0 1] direction. A closer look to the $Rb_2M_6Br_{14}$ structure evidences that it can be described in a pseudo-hexagonal unit-cell with the following cell parameters: $a = 9.072(3)$ Å, $b = 9.757(5)$ Å, $c = 9.169(24)$ Å, $\alpha = 87.39°$, $\beta = 91.40°$, $\gamma = 122.53°$ (Figs. 2a and b). In this pseudo unit-cell, the units are stacked according to a *AAA* arrangement generating distorted prismatic environments of units within which are located the rubidium cations. Rb1 lies at the centre and Rb2 on

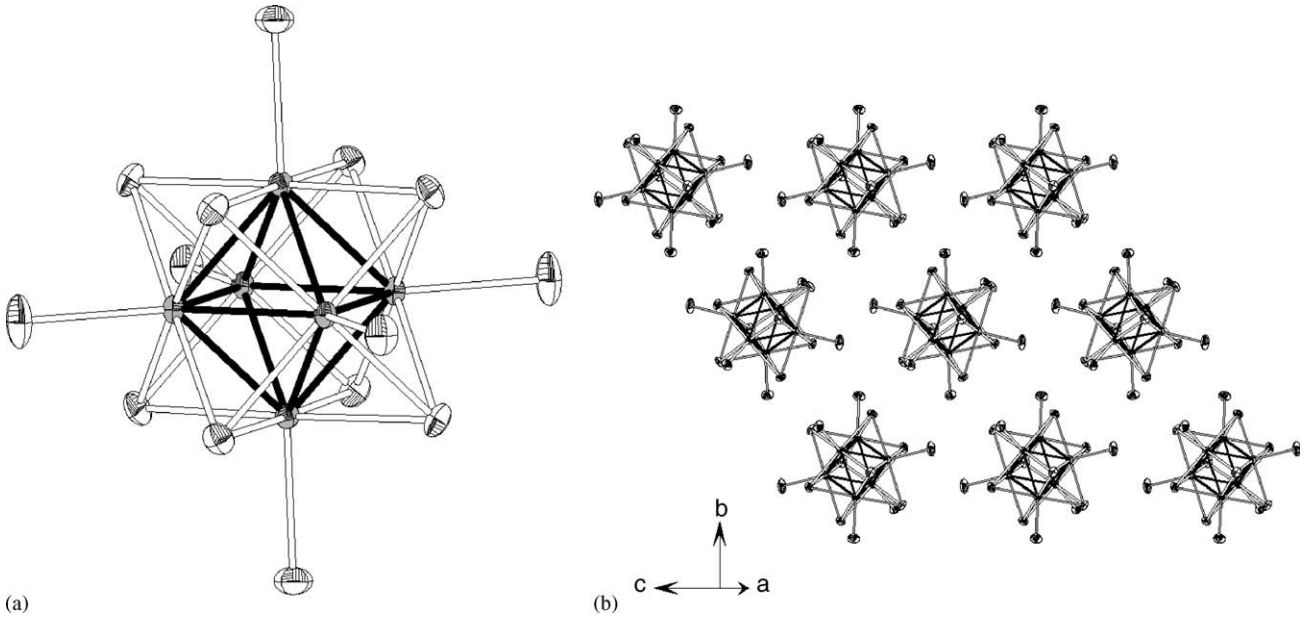

Fig. 1. (a) Mo_6Br_{14} unit. (b) Perpendicular projection of an unit layer in $Rb_2Mo_6Br_{14}$.

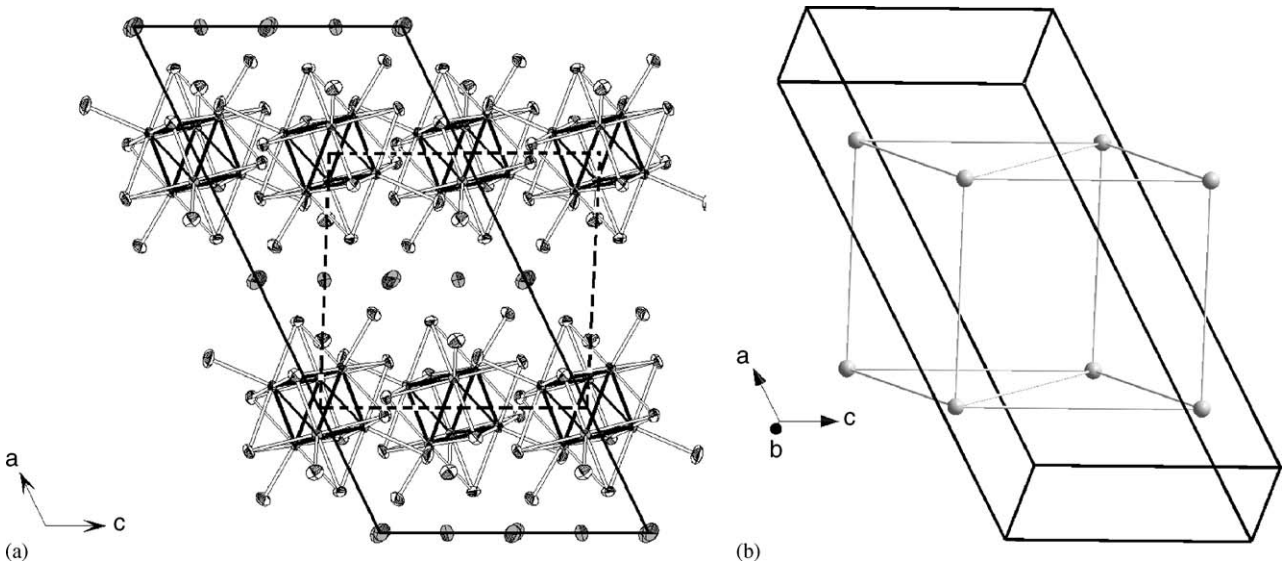

Fig. 2. (a) Projection along the [010] direction, the pseudo-hexagonal unit-cell is represented in dashed lines. (b) Schematic representation of a pseudo-hexagonal unit-cell in $Rb_2Mo_6Br_{14}$. The centroid of cluster is represented as grey balls.

the three parallelepipedic faces of this prismatic site (Figs. 3a and b, respectively). Contrary to $Cs_2Mo_6Br_{14}$ [13] (*P*-31*c*, *ABAB* close-packed hexagonal stacking) in which the ternary axis of the unit is perpendicular to the unit layer, in $Rb_2Mo_6Br_{14}$ the angle between the ternary axis of the unit and the unit layer is equal to 103.16°. This enables closer inter-unit distances within and between the layers in *C*2/*c* structures-types compared to those of other related halides with *Pn*-3 or *P*-31*c* structure-types (see Table 10).

3.2. Crystal structures of $Rb_{2.5}Mo_6Br_{13.5}Te_{0.5}$

The $Rb_{2.5}Mo_6Br_{13.5}Te_{0.5}$ tellurobromide crystallizes in the cubic system (space group *Pn*-3, Fig. 4). Its structure is strongly related to those of $Rb_{2.5}Re_6S_{6.5}Cl_{7.5}$ and $K_{2.5}Re_6S_{6.5}Br_{7.5}$ [10] that are also formulated $(Rb_5)^{5+}[Re_6S^i_6Cl^i_2Cl^a_6]^{2-}[Re_6S^i_7Cl^iCl^a_6]^{3-}$ and $(K_5)^{5+}[Re_6S^i_6Br^i_2Br_6]^{2-}[Re_6S^i_7Br^iBr_6]^{3-}$, respectively. The structure is based on $[Mo_6Br^i_8Br^a_6]^{2-}$ and $[Mo_6Br^i_7Te^iBr^a_6]^{3-}$ discrete anionic units in which the Mo_6 cluster is

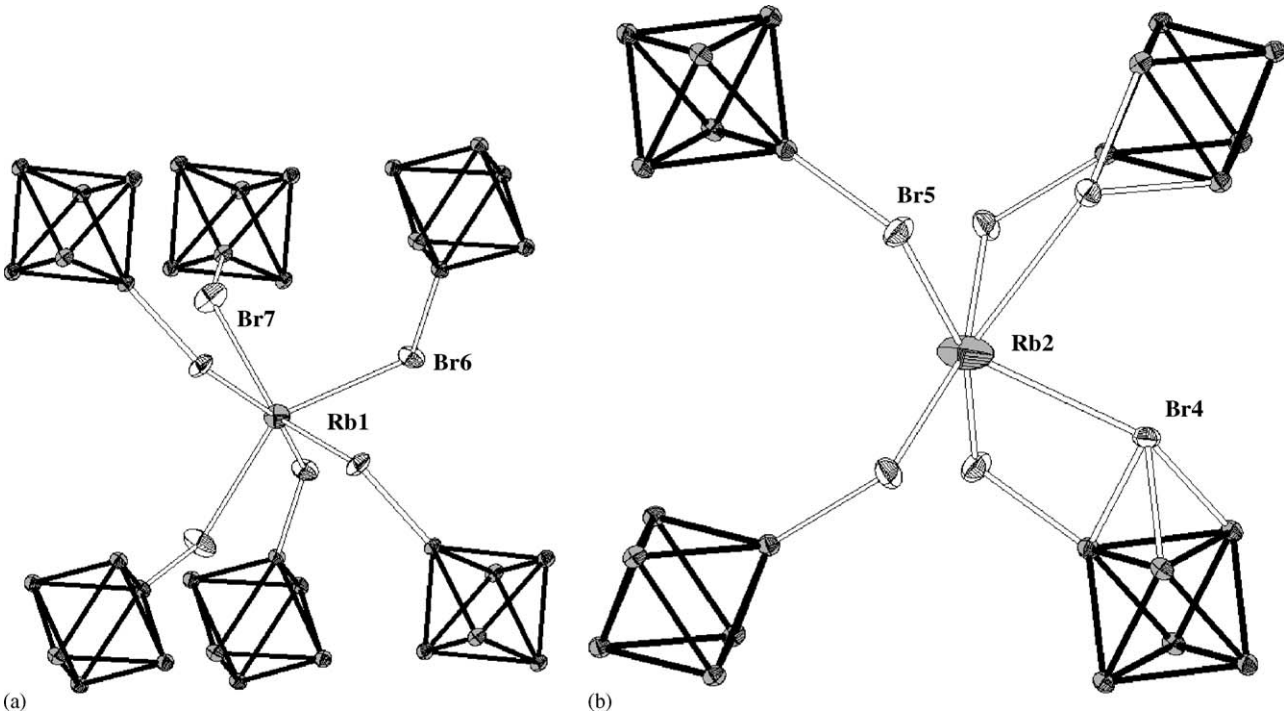

Fig. 3. Rubidium environments. (a) Prismatic environment of unit for Rb1; (b) Rb2 is located on the unit prism faces.

Table 10
Inter-cluster distances in some $A_{2+x}M_6Br^{i}_{8-x}Y^{i}_{x}Br^{a}_{6}$ (Y = Se, Te) compounds according to [11, 13 and this work]

Compound	Space group	Unit diameter Br^{a}–Br^{a} (Å)	Inter-cluster distances (centroid to centroid) within layers (Å)	Inter-cluster distances (centroid to centroid) between layers (Å)
$Rb_2Mo_6Br_{14}$	*C*2/*c*	8.940(16)	9.072(2)–9.757(5)	9.169(24)
$Rb_{2.25}Mo_6Br_{13.75}Se_{0.25}$	*Pn*-3	8.915(17)	9.899(2)	9.899(2)
$Rb_{2.5}Mo_6Br_{13.5}Se_{0.5}$	*Pn*-3	8.953(13)	9.956(3)	9.956(3)
$Rb_{2.7}Mo_6Br_{13.3}Se_{0.7}$	*Pn*-3	8.973(15)	10.001(3)	10.001(3)
$Rb_{2.5}Mo_6Br_{13.5}Te_{0.5}$	*Pn*-3	8.952(16)	9.966(1)	9.966(1)
$Cs_2Mo_6Br_{14}$	*P*-31*c*	8.919(2)	10.192(1)	9.56(1)
$K_2W_6Br_{14}$	*Pn*-3	8.908(2)	9.764(1)	9.764(1)
$Rb_2W_6Br_{14}$	*C*2/*c*	8.926(2)	9.104(1)–9.720(5)	9.159(24)
$Cs_2W_6Br_{14}$	*P*-31*c*	8.907(1)	10.18(1)	9.578(1)

face-capped by eight inner ligands. The average unit is characterized by a random distribution of bromine and tellurium on six inner positions with a Br:Te *ratio* equal to 0.94:0.06. The two other inner ligand positions located on the ternary axis of the unit as well as the apical positions are fully occupied by bromine. Such a distribution implies that the $[Mo_6Br^{i}_7Te^{i}Br^{a}_6]^{3-}$ units are statistically disordered around the three-fold axis of the unit. On the other hand, in $Rb_{2.5}Re_6S_{6.5}Cl_{7.5}$ and $K_{2.5}Re_6S_{6.5}Br_{7.5}$, a random distribution of chalcogen and halogen on all the inner sites has been observed that implies no preferential static disorder.

The layers are arranged according to a *ABC* close-packed cubic stacking along the [111] direction (Fig. 5). Contrary to $Cs_2Mo_6Br_{14}$, for which all the units exhibit their ternary axis perpendicular to the unit layers, in $Rb_{2.5}Mo_6Br_{13.5}Te_{0.5}$, only the units oriented along the [111] direction exhibit their ternary axis perpendicular to the unit layers. The other units are tilted by 45° versus the [111] direction corresponding to an orientation along the [1−11], [−1−11] and [−111] directions. This disposition of units enable equal inter-cluster distances between and within the layers (Table 10). The Rb1 cations are located in the octahedral sites generated by this *ABC* close-packed cubic stacking (4*c* Wyckoff position) whilst Rb2 cations occupy the six over the eight tetrahedral sites (6*d* Wyckoff position). The two remaining tetrahedral sites of units (2*a* Wyckoff position), located on the (111) axis, are unoccupied. Rb1 is bonded to six apical bromine atoms, belonging to six

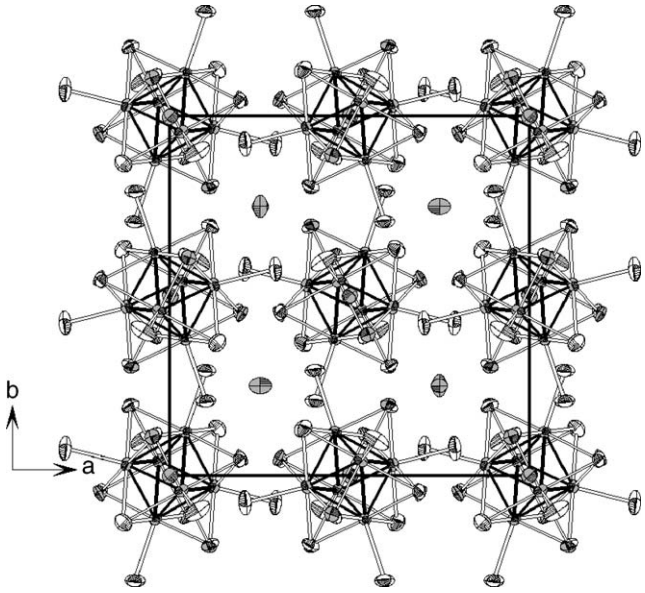

Fig. 4. Projection of the $Rb_3Mo_6Br_{13.5}Te_{0.5}$ structure. The unit-cell is represented in bold.

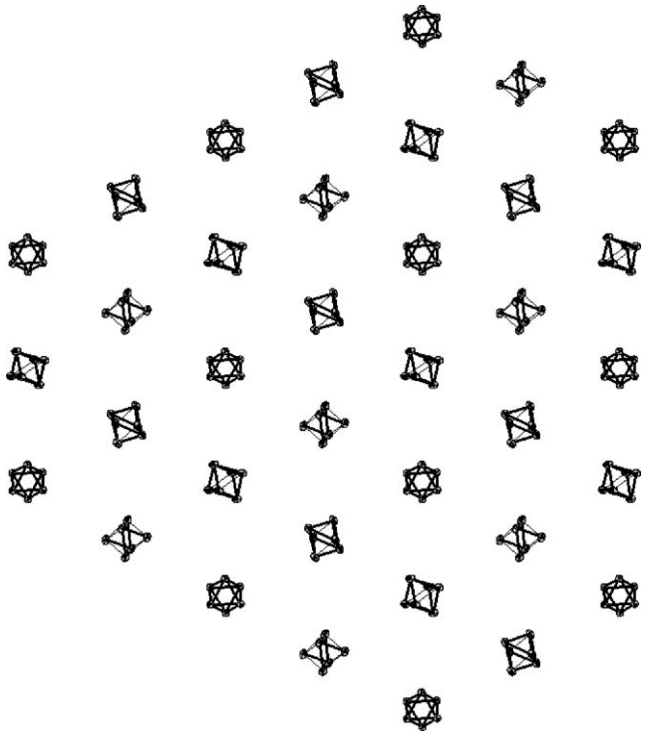

Fig. 5. Projection of an unit layer along the [111] direction.

adjacent Mo_6 clusters, that build a slightly deformed Br_6 octahedron (Fig. 6a, Rb1-Br^a: 3.4043(6) Å). Rb2 is bonded to four apical and four inner bromine atoms belonging to four Mo_6 clusters (Fig. 6b, Rb1-Br^a: 3.3165(7) Å). These Rb–Br^a distances are in agreement with those found in $Rb_2Mo_6Br_{14}$. The Rb2-Br^i and Rb2–Te^i bond lengths are 3.593(2) and 3.53(2) Å, respectively. Owing to the tilting of units, the distance between the centre of the remaining tetrahedral sites (2*a* Wyckoff position) and the four closest Br^i ligands (2.912(1) Å) is too short to enable their occupation by other rubidium cations. Attempts to reach the '$Rb_{2.5}A'_{0.5}Mo_6Br_{13}Te_1$' composition in order to fill the 2*a* site by the use of smaller *A*′ cations, as for instance lithium, have failed.

3.3. Crystal structures of $Rb_{2+x}Mo_6Br^i_{8-x}Se^i{}_xBr^a_6$ series

The structure of $Rb_{2.5}Mo_6Br_{13.5}Se_{0.5}$ is closer to the structures of $Rb_{2.5}Re_6S_{6.5}Cl_{7.5}$ and $K_{2.5}Re_6S_{6.5}Br_{7.5}$ [10] than $Rb_{2.5}Mo_6Br_{13.5}Te_{0.5}$. Indeed, the similar size of Se and Br should favour a random distribution on all inner positions. The analysis of the interatomic distances does not indicate any Se/Br ordering. $Rb_{2.25}Mo_6Br_{13.75}Se_{0.25}$ is characterized by a smaller occupancy of the Rb2 sites compared to $Rb_{2.5}Mo_6Br_{13.5}Se_{0.5}$. Contrary to one could expect first, the additional cations in $Rb_{2.69(1)}Mo_6Br_{13.31(2)}Se_{0.69(2)}$ are not located in the remaining tetrahedral sites of units (2*a* Wyckoff position). Indeed, Rb3 statistically occupies a 8*e* Wyckoff position that corresponds to the triangular sites of units generated within the layers. Closely related triangular environment of units have already been found in $Cs_2Mo_6X_{14}$ halides and related compounds [13]. Attempts to reach '$Rb_{2.5}A'_{0.5}Mo_6Br_{13}Se_1$' by the occupation of 25% (instead of 9.6% in $Rb_{2.69(1)}Mo_6Br_{13.31(2)}Se_{0.69(2)}$) of the 8*e* Wyckoff position using small A′ cations gave unfruitful results.

3.4. Evolution of the interatomic distances

As previously observed for $Cs_4Mo_6Br^i_6Se^i_2Br^a_6$ [3], the replacement of bromine ligands by selenium does not affect significantly the Mo–Mo and Mo–Br^i distances. In other words, the variation of the Mo–Mo and Mo–Br^i bond lengths is not submitted to matrix effect and depends only on the number of valence electrons per cluster. The main difference concerns the Mo–Br^a bond lengths that slightly increase as the average charge of the unit increases. This effect can be related to a lower cationic charge of the $(Mo_6L^i_8)^{n+}$ cluster core (2+ for $Cs_4Mo_6Br_{12}Se_2$ (Mo–Br^a: 2.655 Å); 3.3+ for $Rb_{2.7}Mo_6Br_{13.3}Se_{0.7}$ (Mo–Br^a: 2.6227(8) Å); 3.5+ for $Rb_{2.5}Mo_6Br_{13.5}Se_{0.5}$ (Mo–Br^a: 2.6154(8) Å); 3.75+ for $Rb_{2.25}Mo_6Br_{13.75}Se_{0.25}$ (Mo–Br^a: 2.6019(10) Å); 4+ for $Cs_2Mo_6Br_{14}$ (Mo–Br^a: 2.607 Å)). Indeed, the higher the charge the shorter the Mo–Br^a bond length owing to greater electrostatic interactions.

3.5. Stacking evolution versus anionic charge and counter cations

The analysis of inter-cluster distances (centroid to centroid) reported in Table 10 evidences a higher unit

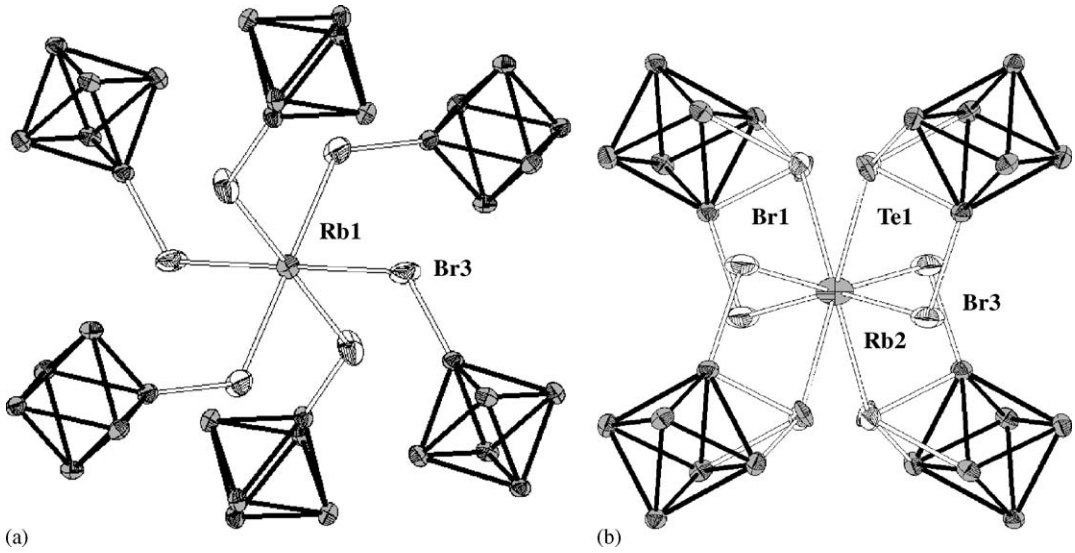

Fig. 6. Rubidium environment in $Rb_{2.5}Mo_6Br_{13.5}Te_{0.5}$. (a) Rb1 octahedral environment of units. (b) Rb2 tetrahedral environment of units.

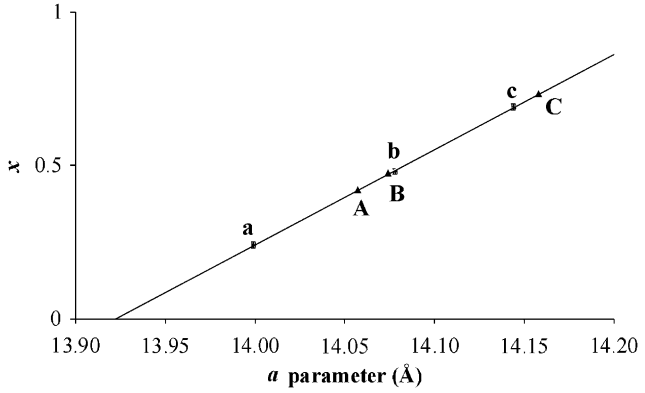

Fig. 7. x values versus refined cell parameters for the $Rb_{2+x}Mo_6Br_{14-x}Se_x$ series. a, b and c correspond to the x value versus a parameter obtained by X-ray single-crystal diffraction data. A, B and C (black triangles) correspond to powder compounds. A, B and C points have been reported on the line previously defined by a, b and c starting from a 'single-crystal' parameters in order to determine the corresponding x value. Standard uncertainties along x and a are included within the symbols.

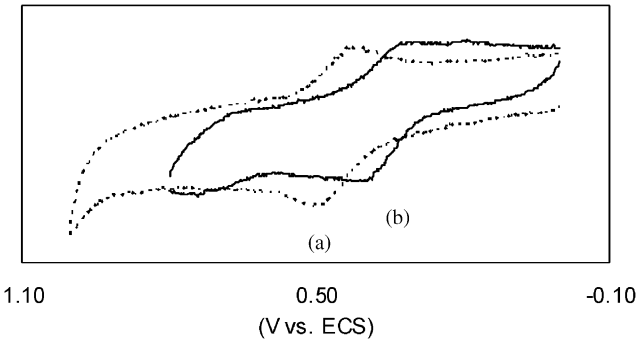

Fig. 8. Cyclic voltammograms of $Rb_{2+x}Mo_6Br^i_{8-x}Y^i_xBr^a_6$ and $Rb_{2.5}Mo_6Br^i_{7.5}Y^i_{0.5}Br^a_6$ series, with $Y = Se$ (a) and $Y = Te$ (b) in dichloromethane/tetrabutylammonium hexafluorophosphate (0.1 M) at $0.5\,V\,s^{-1}$. The ferrocene/ferrocenium (Fc/Fc^+) complex was used as an internal reference for potential measurements (Fc/Fc^+ at 0.460 V vs. SCE).

compactness in the $C2/c$ structure-type. This feature must be related to the tilt of the ternary axis of units within the unit layers. This leads to closer inter-cluster distances within and between the unit layers. Indeed, the crystallization of $Rb_2Mo_6Br_{14}$ in the $C2/c$ structure-type favours a higher space filling compared to a crystallization in the P-31c or Pn-3 structure-types. The replacement of some bromine by selenium ligands involves an increase of the cation content within the structure in order to maintain charge balance in relation with the 24 VEC value. Additional cations cannot be hosted in the $C2/c$ structure-type. As stressed above in the structural results section, the stacking in the Pn-3 structure generates octahedral and tetrahedral sites of units between the layers. Only $\frac{3}{4}$ of the tetrahedral sites can be occupied by cations to reach the $A_{2.5}Mo_6Br_{13.5}Se_{0.5}$ formula. For higher *ratio*, triangular sites within the layers are filled but the '$A_3Mo_6Br_{13}Se_1$' composition has not been reached although it could be obtained by a 25% occupation of these triangular sites. High *ratio* of RbBr and Se in the loaded composition favours the formation of $Rb_4Mo_6Br_{12}Se_2$ or $Rb_{12}Mo_9Br_{31}Se$ together with a significant decrease of the reaction yield of the $Rb_{2+x}Mo_6Br^i_{8-x}Se^i_xBr^a_6$ phase.

3.6. Solution chemistry and electrochemistry

The $A_2Mo_6Br_{14}$ series are hardly soluble in most organic solvents. The $Rb_{2+x}Mo_6Br^i_{8-x}Y^i_xBr^a_6$ series and

Table 11
Oxidation potentials $E_{1/2}$ for selected Mo_6 complexes

		Processes	ΔE_p (V)	i_c/i_a	$E_{1/2}$ (V vs.SCE) [a]
$[Mo_6Br^i_8Br^a_6]^{2-}$	$Cs_2Mo_6Br_{14}$	24/23	/	NR[b]	+1.38
$[Mo_6Br^i_7Se^iBr^a_6]^{3-}$	$Rb_{2+x}Mo_6Br^-_{13-x}Se_x$	24/23	0.09	1	+0.46
$[Mo_6Br^i_7Te^iBr^a_6]^{3-}$	$Rb_{2.5}Mo_6Br_{13.5}Te_{0.5}$	24/23	0.09	1	+0.38
$[Mo_6Br^i_6S^i_2Br^a_6]^{4-}$	$Cs_4Mo_6Br_{12}S_2$	24/23	/	NR[b]	Solvation in solution
$[Mo_6Br^i_6Se^i_2Br^a_6]^{4-}$	$Cs_4Mo_6Br_{12}Se_2$	24/23	/	NR[b]	Solvation in solution
$[Mo_6Br^i_6S^i_2(CN)^a_6]^{4-}$	$Cs_{0.4}K_{0.6}(Et_4N)_{11}[(Mo_6Br_6S_2)(CN)_6]_3\cdot 16H_2O$	24/23	0.09	1	–0.056
$[Mo_6Br^i_6Se^i_2(CN)^a_6]^{4-}$	$Cs_{0.4}K_{0.6}(Et_4N)_{11}[(Mo_6Br_6Se_2)(CN)_6]_3\cdot 16H_2O$	24/23	0.09	1	–0.068

[a]All E values in V vs SCE Conditions: CH_2Cl_2 solvent, 0.1 M $(N^nBu_4)(PF_6)$ supporting electrolyte, 20 °C, Pt electrode, sweep rate 0.100 V s^{-1}. The ferrocene/ferrocenium (Fc/Fc^+) at 0.460 V vs SCE complex was used as an internal reference for potential measurements.
[b]Process not chemically reversible.

$Rb_{2.5}Mo_6Br^i_{7.5}Y^i_{0.5}Br^a_6$ are only sparingly soluble in dichloromethane upon sonication and slightly more in acetonitrile. Beyond the separation of insoluble impurities, their solubility in the former has also allowed to study the electrochemistry of the novel $(Mo_6Br_{13}Se)^{3-}$ and $(Mo_6Br_{13}Te)^{3-}$ anionic units issued from $Rb_{2+x}Mo_6Br^i_{8-x}Se^i_xBr^a_6$ and $Rb_{2.5}Mo_6Br^i_{7.5}Te^i_{0.5}Br^a_6$ solid state precursors. The presence of selenium among the ligands apparently drastically decreases the oxidation potential relative to a $(Mo_6Br_{14})^{2-}$ unit, as already observed in previous work [3 and references therein]. In Table 11, comparison of $E_{1/2}$ of '$Mo_6Br^i_7Se^iBr^a_6$' unit with other Mo_6 units shows that the substitution of inner halogen ligands by chalcogen ones drastically decreases oxidation potentials (for example, +1.38 V for (Mo_6Br_8), +0.55 V for (Mo_6Br_7S) and –0.056 V for $(Mo_6Br_6S_2)$) vs. SCE, whilst the nature of chalcogen (S or Se) itself seems to affect the potential only slightly. In the case of tellurium the oxidation potential is also decreased, leading to a reversible oxidation process centred at 0.38 vs. SCE. Hitherto no isolated mixed tellurium halide Mo_6 units has been reported. In previous work [6–8], mixed sulphur and selenium halide soluble Mo_6 units have been obtained from MoX_2 halide and NaSeH and NaSH. Nothing has been made until the present work on molybdenum tellurium derivatives. Reversible oxidation processes have also been reported for related $[Re_6Te_8L_6]^{4-}$ anionic units [21].

4. Conclusion

The chemistry and the structures of the $Rb_2Mo_6Br^i_8Br^a_6$ bromide and $Rb_{2+x}Mo_6Br^i_{8-x}Y^i_xBr^a_6$ chalcohalides built up from molybdenum octahedral clusters ($x = 0.5$ for $Y = Te$; $0.25 \leqslant x \leqslant 0.7$ for $Y = Se$) have been presented in this work. The crystallochemistry results are based on combined single-crystal and powder X-ray diffraction investigations from several preparations with different loaded compositions. A continuous solid state solution has been evidenced between the two compositions $Rb_{2.25}Mo_6Br_{13.75}Se_{0.25}$ and $Rb_{2.7}Mo_6Br_{13.3}Se_{0.7}$. On the other hand, in the case of tellurium no solid state solution has been observed as previously reported for $Rb_{2.5}Re_6S_{6.5}Cl_{7.5}$ and $K_{2.5}Re_6S_{6.5}Br_{7.5}$. The electrochemistry performed on the $[Mo_6Br_{13}Y]^{3-}$ units reveals a reversible 24/23 electrons process with $E_{1/2} =$ 0.46 and 0.38 V vs. SCE for $[Mo_6Br_{13}Se]^{3-}$ and $[Mo_6Br_{13}Te]^{3-}$, respectively.

Acknowledgments

We are indebted to the French Research Ministry for 'ACI Nanosciences 2001—No. 18-01' contract and to "Fondation Langlois" for financial support.

Appendix A. Supplementary materials

The online version of this article contains additional supplementary data. Please visit doi:10.1016/j.jssc.2005.07.026

References

[1] H. Schäfer, H.-G.V. Schnering, Angew. Chem. 76 (1964) 833.
[2] C. Perrin, S. Cordier, S. Ihmaine, M. Sergent, J. Alloy Compd. 229 (1995) 123.
[3] S. Cordier, N. Naumov, D. Salloum, F. Paul, C. Perrin, Inorg. Chem. 43 (2004) 219.
[4] (a) C.B. Gorman, W.Y. Su, H. Jiang, C.M. Watson, P. Boyle, Chem. Commun. (1999) 877
(b) D. Méry, L. Plault, S. Nlate, D. Astruc, S. Cordier, K. Kirakci, C. Perrin, Z. Anorg. Allg. Chem. (2005), in press.
[5] N. Naumov, A.V. Virovets, V.E. Fedorov, J. Struct. Chem. 41 (2000) 499.
[6] J.B. Michel, R.E. McCarley, Inorg. Chem. 21 (1982) 1864.
[7] (a) M. Ebihara, K. Toriumi, K. Saito, Inorg. Chem. 27 (1988) 13;
(b) A.W. Maverick, J.S. Najdzionek, D. MacKenzie, D.G. Nocera, H.B. Gray, J. Am. Chem. Soc. 105 (1983) 1878.
[8] M. Ebihara, K. Isobe, Y. Sasaki, K. Saito, Inorg. Chem. 31 (1992) 1644.
[9] J.C. Gabriel, K. Boubekeur, P. Batail, Inorg. Chem. 32 (1993) 2894.

[10] A. Slougi, Thesis of the Rennes 1 University, 1998, No. 2026.
[11] Y.Q. Zheng, K. Peters, Y. Grin, H.G. von Schnering, Z. Anorg. Allg. Chem. 624 (1998) 506.
[12] H. Schäfer, H.G. von Schnering, J. Tillack, F. Kuhnen, H. Wöhrle, H. Baumann, Z. Anorg. Allg. Chem. 353 (1967) 281.
[13] K. Kirakci, S. Cordier, C. Perrin, Z. Anorg. Allg. Chem. 631 (2005) 411.
[14] A.J.M. Duisenberg, L.M.J. Kroon-Batenburg, A.M.M. Schreurs, J. Appl. Crystallogr. 36 (2003) 220.
[15] G.M. Sheldrick, SADABS Version 2.03, Bruker AXS Inc., Madison, Wisconsin, USA, 2002.
[16] R.E. Marsh, Acta Crystallogr. B 51 (1999) 897.
[17] A. Altomare, M.C. Burla, M. Camalli, G. Cascarano, C. Giacovazzo, A. Guagliardi, A.G.G. Moliterni, G. Polidori, R. Spagna, J. Appl. Crystallogr. 32 (1999) 115.
[18] G.M. Sheldrick, SHELXL-97: Program for the Refinement of Crystal Structure, University of Göttingen, Göttingen, 1997.
[19] R.P. Shannon, Acta Crystallogr. A 32 (1976) 751.
[20] (a) C. Perrin, M. Sergent, J. Less Common Metals 123 (1986) 117;
(b) A. Perrin, C. Perrin, M. Sergent, J. Less Common Metals 137 (1988) 241.
[21] P. Thompson, D.E. Cox, J.B. Hastings, J. Appl. Crystallogr. 20 (1987) 79–83.
[22] J. Rodriguez-Carvajal, "FULLPROF: A Program for Rietveld Refinement and Pattern Matching Analysis", Abstracts of the Satellite Meeting on Powder Diffraction of the XV Congress of the IUCr, Toulouse, France, 1990, p. 127.
[23] T. Roisnel, J. Rodríguez-Carvajal, WinPLOTR: a Windows tool for powder diffraction patterns analysis Materials Science Forum, in: R. Delhez, E.J. Mittenmeijer (Eds.), Proceedings of the Seventh European Powder Diffraction. Conference (EPDIC 7), 2000, pp. 118–123.
[24] K. Kirakci, et al., The $Rb_{12}Mo_9Br_{31}Y$ series (cubic, *Pm*-3*m*) are based on monosubstituted Mo_6 cluster units and $Mo^{III}Br_6^{3-}$ entities, in progress.
[25] J.C.P. Gabriel, K. Boubekeur, S. Uriel, P. Batail, Chem. Rev. 101 (2001) 2037.
[26] M. Potel, C. Perrin, A. Perrin, M. Sergent, Mater. Res. Bull. 21 (1986) 1239.